Pflugers Arch - Eur J Physiol (2006) 452: 396–406
DOI 10.1007/s00424-006-0046-9

Patrick Bader · Robert Weingart

Pitfalls when examining gap junction hemichannels: interference from volume-regulated anion channels

Received: 21 December 2005 / Accepted: 5 January 2006 / Published online: 8 April 2006

Abstract Human HeLa cells transfected with mouse connexin45 were used to explore the experimental conditions suitable to measure currents carried by gap junction hemichannels. Experiments were performed with a voltage-clamp technique and whole-cell recording. Lowering $[Ca^{2+}]_o$ from 2 mM to 20 nM evoked an extra current, I_m, putatively carried by Cx45 hemichannels. However, the variability of I_m (size, voltage sensitivity, kinetics) suggested the involvement of other channels. The finding that growth medium in the incubator increased the osmolarity with time implied that volume-regulated anion channels (VRAC) may participate. This assumption was reinforced by the following observations. On the one hand, keeping $[Ca^{2+}]_o$ normal while the osmolarity of the extracellular solution was reduced from 310 to 290 mOsm yielded a current characteristic of VRAC; I_{VRAC} activated/deactivated at negative/positive voltage, giving rise to the conductance functions $g_{VRAC,inst}=f(V_m)$ (inst: instantaneous; V_m: membrane potential) and $g_{VRAC,ss}=f(V_m)$ (ss: steady state). Moreover, it was reversibly inhibited by mibefradil, a Cl^-channel blocker (binding constant K_d=38 μM, Hill coefficient n=12), but not by the gap junction channel blocker 18α-glycyrrhetinic acid. On the other hand, minimizing the osmotic imbalance while $[Ca^{2+}]_o$ was reduced led to a current typical for Cx45 hemichannels; I_{hc} activated/deactivated at positive/negative voltage. Furthermore, it was reversibly inhibited by 18α-glycyrrhetinic acid or palmitoleic acid, but not by mibefradil. Computations based on $g_{VRAC,ss}=f(V_m)$ and $g_{hc,ss}=f(V_m)$ indicated that the concomitant operation of both currents results in a bell-shaped conductance–voltage relationship. The functional implications of the data presented are discussed. Conceivably, VRAC and hemichannels are involved in a common signaling pathway.

P. Bader · R. Weingart (✉)
Department of Physiology,
University of Bern,
Bühlplatz 5,
CH-3012 Bern, Switzerland
e-mail: weingart@pyl.unibe.ch
Tel.: +41-031-6318706
Fax: +41-031-6314611

Keywords Gap junction hemichannel · Connexin45 · Volume-regulated anion channel · Electrophysiology · Pharmacology

Introduction

Gap junctions are aggregates of channels offering a direct pathway for the exchange of ions and small molecules between adjoining cells. Each channel consists of two hemichannels in series, and each hemichannel (connexon) is made of six subunits (connexins) forming an aqueous pore. Gap junctions are dynamic structures [23]. Formation of their channels involves docking of preformed hemichannels located in the cell membrane of adjacent cells; breakdown of channels occurs via endocytosis and degradation.

Cell pairs are suitable for studying gap junction channels with a dual voltage-clamp technique (see [13]). It enables one to determine the conductive and kinetic channel properties. Single cells are convenient for examining hemichannels with a single voltage-clamp method [28]. It allows one to assess the respective properties of hemichannels and gain insight into functional aspects of gap junction channels not accessible to cell-pair studies. Solitary hemichannels embedded in cell membranes are usually closed under physiological conditions. To study their properties, they have to be opened using specific experimental protocols, i.e. lowering $[Ca^{2+}]_o$ or altering the membrane potential (see [13]). When examining the electrical properties of hemichannels, a potential problem is the interference from other channels. Various preparations have been used in the past to examine hemichannels, e.g. isolated primary cells [7, 14], injected oocytes [10, 26] or transfected cell lines [2, 16, 27, 28]. In some cases, the measures taken to limit the contribution of other channels may have been scant. Recent evidence suggests that hemichannels residing in cell membranes can be opened under physiological or pathophysiological conditions [14, 15, 24].

In this study, we have optimized the conditions to determine the electrical properties of hemichannels using

cells with a high input resistance and solutions with channel blockers to minimize interference from other currents. For this purpose, we have used HeLa cells transfected with mouse Cx45. They possess a limited selection of intrinsic channels, i.e. potassium channels [8, 21, 22] and a chloride channel [9, 19, 22]. It turned out that small osmotic disturbances are sufficient to activate an extra current. Electrophysiological and pharmacological experiments indicated that this current is carried by volume-regulated anion channels (VRAC). Since its properties are mirror images of those of hemichannel currents, caution is required when examining the latter. A preliminary report has been published before [1].

Methods

Cells and culture conditions

Human HeLa cells transfected with cDNA coding for mouse connexin45 [11] and wild-type HeLa cells were grown in DMEM containing 10% FCS, 100 μg/ml streptomycin and 100 U/ml penicillin. Transfectants were selected with 0.5–1 μM puromycin (Sigma). For experiments, the cells were harvested in DMEM containing 10% FCS (~0.2×10^6 to 10^6 cells/ml) and seeded onto sterile glass coverslips placed in culture dishes (~10^4 cells/cm^2). Electrical measurements were performed 1–2 days later.

Solutions

Experiments were carried out in KCl-rich solution containing normal Ca^{2+} [in millimolar: KCl, 140; NaCl, 4; $CaCl_2$, 2; $MgCl_2$, 1; HEPES, 5 (pH 7.4); glucose, 5; pyruvate, 2; $CsCl_2$, 2; $BaCl_2$, 1; TEA^+–Cl^-, 2] or low Ca^{2+} [in millimolar: $CaCl_2$, 1; EGTA, 5 (free Ca^{2+} ~20 nM or pCa=7.7)]. Patch pipettes were filled with pipette solution [in millimolar: KCl, 140; NaCl, 4; $CaCl_2$, 1; $MgCl_2$, 1; MgATP, 3; HEPES, 5 (pH 7.2); EGTA, 5 (free Ca^{2+} ~45 nM or pCa=7.4); $CsCl_2$, 2; $BaCl_2$, 1; TEA^+ Cl^-, 2]. Ba^{2+}, Cs^+ and TEA^+ were added to block K^+ currents. To prepare stock solutions, 18α-glycyrrhetinic acid (G-8503; Sigma) and palmitoleic acid (P-9417; Sigma) were dissolved in DM SO (20 mM) and hexane (20 mM), respectively; mibefradil (gift from La Roche, Basel, Switzerland) was dissolved in H_2O (20 mM). Initially, the osmolarity of the salt solutions was not adjusted (see "Initial observations" in "Results"). Later on, this was done by adding mannitol. The osmolarity of growth medium was 310 mOsm and served as standard. Osmolarity was measured with an osmometer (3MO; Advanced Instruments, Needham Heights, MA, USA).

Electrical measurements

Coverslips with adherent cells were transferred to an experimental chamber mounted on an inverted microscope (Diaphot-TMD; Nikon, Nippon Kogaku, Tokyo, Japan). The chamber was superfused with Ca^{2+}-containing solution at room temperature (22–25°C). Patch pipettes were pulled from glass capillaries (GC150F-10; Harvard Apparatus, Edenbridge, UK) with a horizontal puller (DMZ-Universal; Zeitz Instruments, Augsburg, Germany). To reduce capacitance, the pipette tips were coated with silicon elastomer (Sylgard 184; Dow Corning, Wiesbaden, Germany). When filled with solution, the pipettes had DC resistances of 3–5 MΩ. Experiments were carried out on single cells using a voltage-clamp method and whole-cell recording [28]. Patch pipettes connected to an amplifier (EPC 7; HEKA Elektronik, Lambrecht/Pfalz, Germany) were manoeuvred with a micromanipulator (MP-258; Sutter Instrument, Novato, CA, USA).

Signal recording and analysis

The signals were filtered at 1 kHz (8-pole Bessel) and digitized at 3 kHz (ITC-16; Instrutech, Port Washington, NY, USA). Data acquisition and analysis were done with PULSE/PULSFIT (HEKA Elektronik), curve fitting and statistical analysis with SigmaPlot and SigmaStat (Jandel Scientific, Erkrath, Germany), respectively.

Results

Initial observations

After establishing the whole-cell recording condition in solution containing normal Ca^{2+}, the bath was superfused with low-Ca^{2+} solution. In transfected HeLa cells, this was expected to elicit a current carried by Cx45 hemichannels [2]. The extra current observed varied considerably. In some cells, it was significant, in others marginal. This may reflect a change in Cx45 expression during the cell cycle [3]. However, in some cells, the extra current showed a time-dependent decay at negative V_m, in others at positive V_m (Fig. 1). Starting from a holding potential V_h=0 mV, V_m was first depolarized (prepulse) and then hyperpolarized (test pulse) or vice versa. Figure 1a shows a cell whose I_m increased slightly with time at positive voltage (V_m=30 mV) and decayed significantly with time at negative voltage (V_m=−40 mV). Conversely, Fig. 1b shows a cell whose I_m increased marginally at negative voltage (V_m=−90 mV) and declined prominently at positive voltage (V_m=90 mV). In both cases, prior to the intervention, I_m was small and time-independent (superimposed traces). The diverse behaviour of I_m may indicate the presence of two types of connexins. However, this possibility can be ruled out. Immunohistochemistry has revealed that wild-type HeLa cells express the same connexin as the transfectants examined, i.e. Cx45, but at negligible level [11].

In some transfectants, currents similar to those in Fig. 1b already developed in solution with normal Ca^{2+}. Yet, it is generally thought that hemichannels are closed under this condition. Moreover, some wild-type HeLa cells showed such currents in low-Ca^{2+} solution. This would be con-

sistent with the report that pairs of these cells exhibit intercellular currents attributable to intrinsic Cx45 [30]. However, their low incidence renders it unlikely.

To solve the puzzle, an involvement of other channels was considered. HeLa cells have two types of inwardly rectifying K^+ channels of low unitary conductance [8, 21, 22]. However, interference from these channels could be excluded because the solutions contained blocking agents such as Cs^+, TEA^+ and Ba^{2+} (see [28]). Searching for other channels, we have measured the osmolarity of the solutions. A key finding was that fresh and used growth medium showed a different osmolarity. It increased by ~6% in 48 h in the incubator, despite the water-saturated atmosphere. Hence, switching from growth medium to salt solutions imposed an osmotic imbalance, suggesting the interference from VRAC ([9, 19]; see also [18]).

Volume-regulated anion channels

To explore the involvement of VRAC, the medium in the culture dishes was replaced by fresh medium 2–3 h prior to an experiment. This enabled the cells to readjust to the reference osmolarity, thus avoiding osmotic effects when transferring cells to the experimental chamber. Transfected HeLa cells pretreated in this way failed to develop an extra current in solution with normal Ca^{2+}. However, when superfused with low-Ca^{2+} solution, an extra current developed persistently comparable to that in Fig. 1a.

Next, the focus was on salt solutions. The salines with normal and low Ca^{2+} as well as the pipette solution were adjusted to the reference osmolarity to minimize osmotic shifts when changing solution. The growth medium in the culture dishes was again replaced prior to the use of cells. After a control period of 1 min, the solution with normal Ca^{2+} and osmolarity was replaced by solution with normal Ca^{2+} but reduced osmolarity (290 mOsm). During control, hyperpolarization and depolarization led to a small constant inward and outward current, respectively. During the intervention, an extra current evolved with an increasing inward and a decreasing outward component, respectively, similar to that in Fig. 1b. Figure 2 illustrates the development of the extra current, plotting as a function of time the amplitude of the maximal inward current, $I_{VRAC,max}$ (△) the instantaneous outward current, $I_{VRAC,inst}$ (○), and the steady-state outward current, $I_{VRAC,ss}$ (●). Since this current was induced by osmotic disturbance, it is likely to be carried by VRAC. Because it vanished after osmotic adjustment of the growth medium and the salt solutions, it cannot be serum-mediated.

Pharmacology of I_{VRAC}

Pharmacological experiments were done to further qualify the current induced by osmotic changes. Mibefradil, a VRAC blocker, seemed appropriate for this purpose [18, 20]. Figure 3 illustrates an experiment. The bipolar pulse protocol (see Fig. 1b) was applied every 30 s. At time t=0 min, the osmolarity of the solution was reduced from 310 to 290 mOsm. Shortly after the intervention, the three current components begun to grow; $I_{VRAC,max}$ (△) and $I_{VRAC,inst}$ (○) increased significantly, $I_{VRAC,ss}$ (●) marginally. Exposure to 40 μM mibefradil at time t=5 min reduced $I_{VRAC,max}$ (△) and $I_{VRAC,inst}$ (○). Upon washout of the blocker at t=10 min, the current components increased again. During the intervention, $I_{m,ss}$ (●) underwent a small maintained increase which may reflect a minor leak. The incomplete recovery of $I_{VRAC,max}$ (△) and $I_{VRAC,inst}$ (○) during washout of mibefradil and their increase beyond the level prior to the intervention are consistent with this explanation. Four additional experiments yielded similar results. They suggest that the extra current was carried by VRAC.

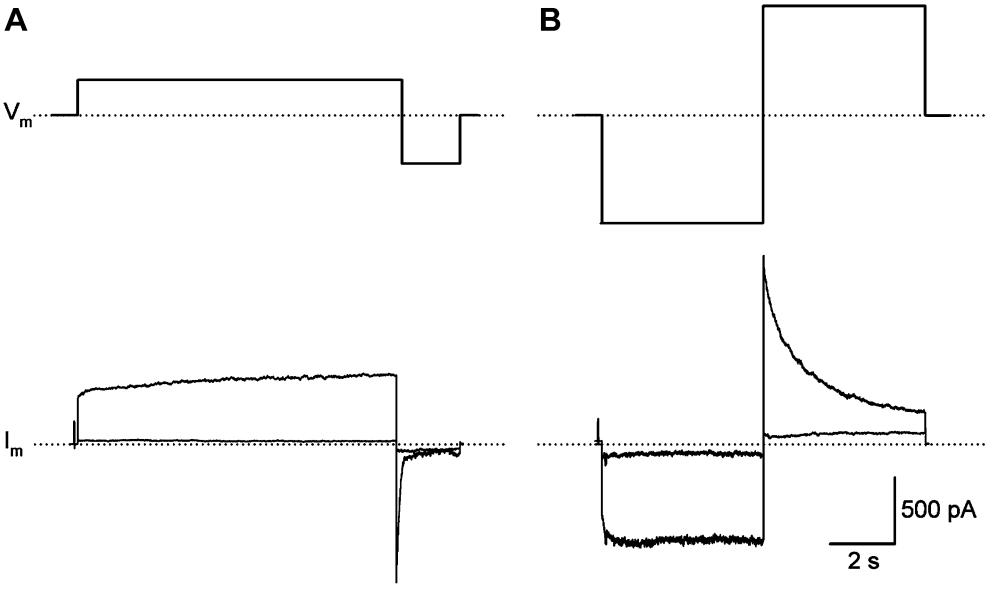

Fig. 1 Recruitment of extra currents. **a** *Upper panel*: pulse protocol. Starting from 0 mV, V_m was depolarized to 30 mV for 10 s (prepulse), then hyperpolarized to −40 mV for 2 s (test pulse). *Lower panel*: currents I_m in control solution (small signal) and after 5 min in low-Ca^{2+} solution (large signal). **b** *Upper panel*: pulse protocol. V_m was hyperpolarized to −90 mV for 5 s, then depolarized to 90 mV for 5 s. *Lower panel*: currents I_m in control solution (small signal) and after ~5 min in low-Ca^{2+} solution (large signal)

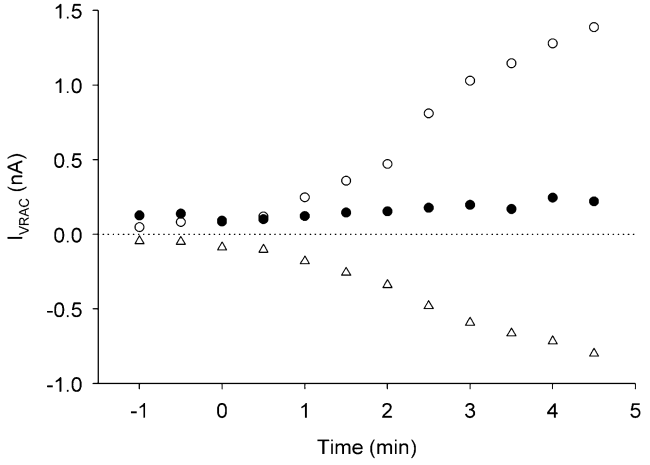

Fig. 2 Effects of osmolarity on recruitment of extra currents putatively carried by VRAC. A bipolar voltage pulse (prepulse: −90 mV, 5 s; test pulse: 90 mV, 5 s) was applied every 30 s. At time t=0 min, solution with normal Ca^{2+} (2 mM) and of normal osmolarity (310 mOsm) was replaced by solution of reduced osmolarity (290 mOsm). △, $I_{m,max}$ (maximal inward current associated with prepulse); ○, $I_{VRAC,inst}$ (instantaneous outward current at beginning of test pulse); ●, $I_{VRAC,ss}$ (steady-state outward current at end of test pulse)

To quantify the effects of mibefradil on I_{VRAC}, a dose–response curve was established. The amplitude of $I_{VRAC,max}$ was determined at different mibefradil concentrations. Each preparation was exposed to control solution and to one or several [mibefradil]. The values of $I_{VRAC,max}$ gathered from each preparation were converted to conductances, $g_{VRAC,max}$, and normalized to the conductance in control solution. The normalized values were averaged and plotted vs log [mibefradil] (Fig. 4). The smooth curve corresponds to the best fit of data to the equation

$$g_{VRAC} = \frac{1}{(1 + (K_d/[mibefradil])^n)}, \quad (1)$$

for the following parameters: K_d=38 μM (binding constant), n=12 (Hill coefficient). Complementary experiments revealed that I_{VRAC} is not affected by 40 μM 18α-glycyrrhetinic acid and barely reduced by 50 μM palmitoleic acid (12±2.7%, n=8), doses fully blocking gap junction hemichannels (see "Pharmacology of I_{hc}").

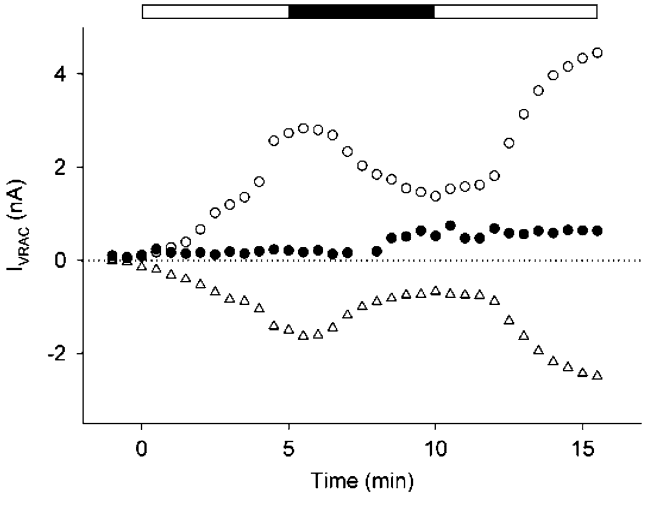

Fig. 3 Pharmacological identification of currents putatively carried by VRAC. Time-course study of current components. △, $I_{VRAC,max}$ (maximal inward current associated with prepulse); ○, $I_{VRAC,inst}$ (instantaneous outward current at beginning of test pulse); ●, $I_{VRAC,ss}$ (steady-state outward current at end of test pulse). Interventions: time t=0 min, reduction in osmolarity of bath solution from 310 to 290 mOsm; t=5 min, addition of 40 μM mibefradil; t=10 min, washout of mibefradil

Voltage sensitivity of I_{VRAC}

To study the voltage dependence of I_{VRAC}, cells were subjected to the same osmotic intervention (see above). Starting from V_h=0 mV, V_m was hyperpolarized to −90 mV for 3 s and then depolarized to different levels for 5 s at increments of 10 mV (Fig. 5a). The prepulse served to evoke a maximal I_{VRAC}, the test pulse to study the voltage dependence. Figure 5b shows a family of records. The induced current showed a distinct deactivation at positive V_m. For analysis, the amplitudes of $I_{VRAC,inst}$ and $I_{VRAC,ss}$ were determined at the beginning and end of each test pulse. Figure 5c illustrates the current–voltage relationships. Over the V_m range examined, $I_{VRAC,inst}$ (○) showed a slight outward rectification with a curved segment at negative voltage and a nearly linear segment at positive voltage (conductance 18.6 nS). In contrast, $I_{VRAC,ss}$ (●) showed a prominent decline at voltages above 30 mV.

Figure 6a illustrates the normalized functions $g_{VRAC,inst}=f(V_m)$ (○) and $g_{VRAC,ss}=f(V_m)$ (●) summarizing the data from four cells. To normalize the $g_{VRAC,inst}$ data, the conductance extrapolated to V_m=0 mV was used as reference. It was obtained by averaging the values of $g_{VRAC,inst}$ at V_m=±

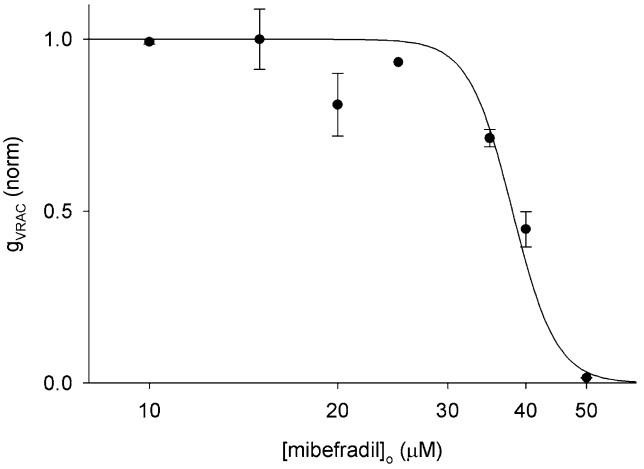

Fig. 4 Dose–response relation for I_{VRAC} vs mibefradil concentration. Normalized changes in I_{VRAC} were averaged and plotted against [mibefradil] on log scale. *Symbols* correspond to mean values±1 SEM (n=11). Continuous curve: least-squares fit of data to Hill equation: K_d=38 μM (binding constant), n=12 (Hill coefficient)

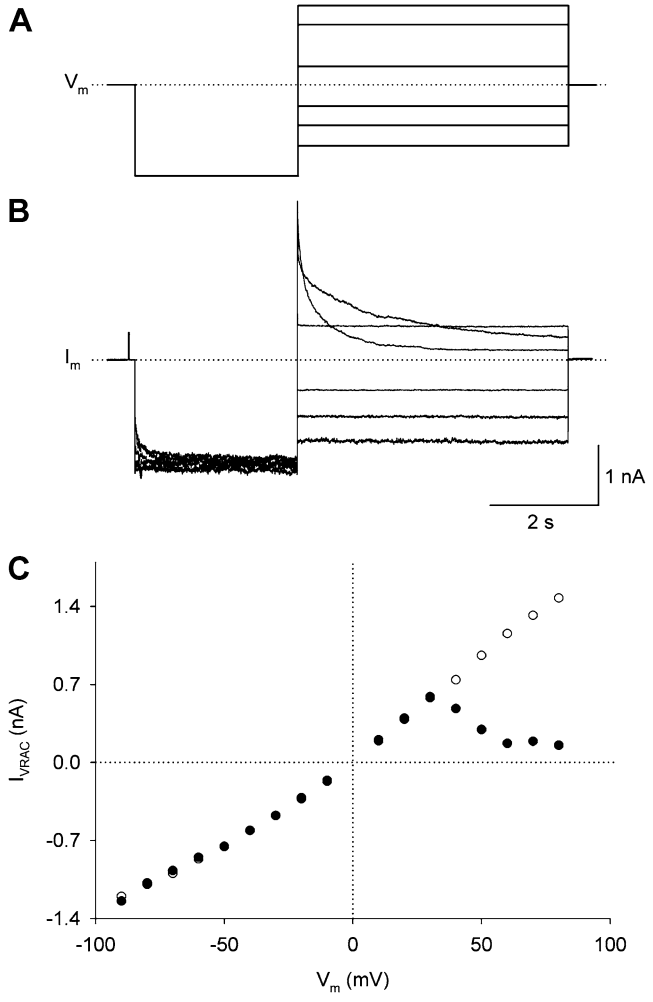

Fig. 5 Voltage dependence of currents carried by VRAC. **a** Bipolar pulse protocol consisting of a hyperpolarizing prepulse from 0 to −90 mV for 3 s, followed by a variable test pulse to negative (−60, −40 and −20 mV) and positive voltages (20, 70 and 90 mV) for 5 s. **b** Family of current traces, I_{VRAC}. The prepulse resulted in an inward current. Test pulses to negative V_m gave rise to inward currents of constant amplitude; test pulses to positive V_m led to outward currents decaying with time. **c** Plot of instantaneous current, $I_{VRAC,inst}$ (○), and steady-state current, $I_{VRAC,ss}$ (●), against V_m prevailing during test pulses

10 mV. To normalize the $g_{VRAC,ss}$ data, the values of $g_{VRAC,ss}$ were expressed as fraction of $g_{VRAC,inst}$ during a pulse. The plot $g_{VRAC,inst}=f(V_m)$ hinted a sigmoidal relationship with a maximum at positive and a minimum at negative V_m, giving rise to a shallow transition with a positive slope. The plot $g_{VRAC,ss}=f(V_m)$ yielded a pronounced sigmoidal relationship with a maximum at negative and a minimum at positive V_m, leading to a steep transition with a negative slope. The smooth curve represents the best fit of data to the Boltzmann equation (see [29]):

$$\frac{g_{ss}}{g_{inst}} = \frac{g_{max} - g_{min}}{1 + e^{[A(V_m - V_{m,0})]}} + g_{min}. \quad (2)$$

The analysis yielded the following parameters: $V_{VRAC,0}$=39.9 mV (V_m at which $g_{VRAC,ss}$ is half-maximally deactivated), $g_{VRAC,max}$=1.01 (maximal value of $g_{VRAC,ss}$), $g_{VRAC,min}$=0.18 (minimal value of $g_{VRAC,ss}$), A=0.32 (constant expressing gating charge), z=8.1 (unitary positive charge q moving through the electric field applied; $A=zq(kT)^{-1}$; k, Boltzmann constant; T, temperature in Kelvin).

VRAC currents were also studied in the presence of pipette solution containing K^+ aspartate$^-$ instead of KCl. This resulted in a shift of the reversal potential from 0.5± 0.9 to 22.5±3.7 mV (n=5), indicating that the channels are less permeable to aspartate$^-$ than Cl^-.

Kinetics of I_{VRAC}

The current records in Fig. 5b were also used to analyse the time-course of I_{VRAC} deactivation. A least-square curve-fitting indicated that I_{VRAC} decreases exponentially with

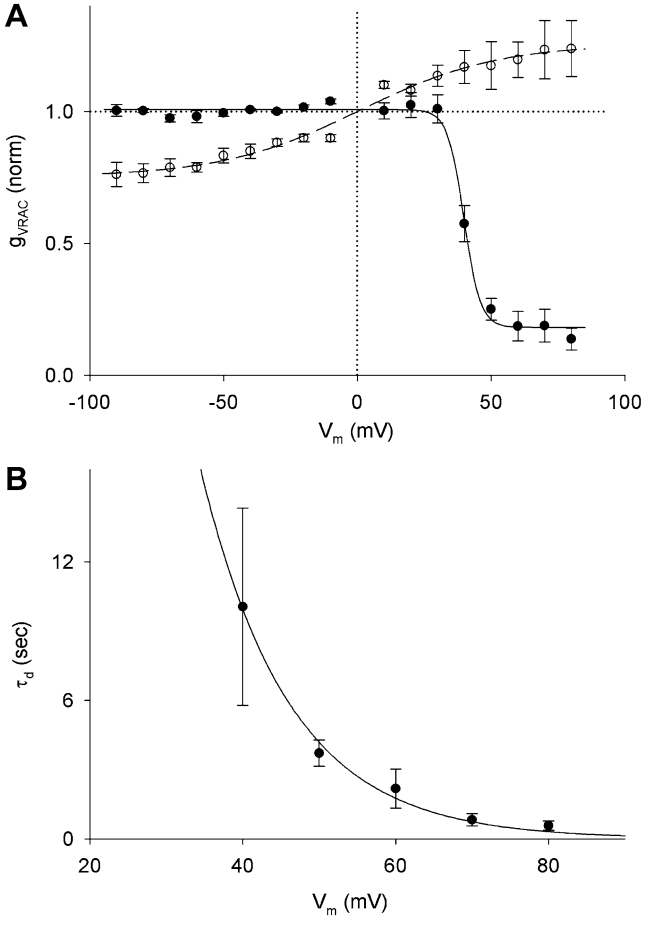

Fig. 6 Conductance and kinetic properties of VRAC. **a** Plot of instantaneous conductance, $g_{VRAC,inst}$ (○), and steady-state conductance, $g_{VRAC,ss}$ (●), against V_m. *Symbols* correspond to mean values± SEM (n=4). Continuous curve: least-squares fit of data to Eq. 2: $V_{VRAC,0}$=39.9 mV, $g_{VRAC,max}$=1.01, $g_{VRAC,min}$=0.18, z=8.1. **b** Plot of time constant of I_{VRAC} deactivation, τ_d, against V_m. Continuous curve: least-squares fit of data to Eq. 3: $\tau_{d,0}$=317 s (zero V_m intercept), V_τ = 11.6 mV (decay constant)

time (not shown). Figure 6b shows the analysis plotting the time constants of deactivation, τ_d, as function of V_m. Over the voltage range examined, τ_d decreased steeply as V_m was made more positive. The smooth curve corresponds to the best fit of data to an exponential,

$$\tau_d = \tau_{d,0} \cdot e^{-\frac{V_m}{V_\tau}}, \quad (3)$$

using the following parameters: $\tau_{d,0}$=317 s (zero V_m intercept), $V_\tau = 11.6$ mV (decay constant).

Gap junction hemichannels

Currents putatively carried by Cx45 hemichannels, I_{hc}, were elicited in solution with low Ca^{2+}. The following precautions were taken to minimize the interference from I_{VRAC}: (1) adjustment of the osmolarity of each solution to 310 mOsm and (2) addition of 60 μM mibefradil to the bath solution. The currents were studied with a bipolar pulse protocol. Starting from V_h=0 mV, V_m was depolarized to 30 mV for 10 s and then hyperpolarized to −40 mV for 5 s. This yielded current signals similar to that in Fig. 1a. Figure 7 illustrates the recruitment of the extra current plotting the amplitude of the maximal outward current $I_{hc,max}$ (△), the instantaneous inward current $I_{hc,inst}$ (○) and the steady-state inward current $I_{hc,ss}$ (●). The extra current was absent in wild-type HeLa cells, suggesting that it is carried by Cx45 hemichannels [2].

Pharmacology of I_{hc}

I_{hc} was further qualified by exposure to palmitoleic acid, a gap junction channel blocker [4]. After a control period, i.e. at time t=0 min, the extracellular Ca^{2+} concentration was reduced to elicit an I_{hc}. Figure 8 illustrates an experiment. The amplitude of $I_{hc,max}$ (△), $I_{hc,inst}$ (○) and $I_{hc,ss}$ (●) increased gradually. At time t=7 min, 50 μM palmitoleic acid was applied. This led to a complete inhibition of the extra current. At time t=11 min, the blocking agent was washed out. To speed up the recovery, 1 mg/ml albumin was added to the washout solution to trap the fatty acid. The amplitude $I_{hc,max}$ and $I_{hc,ss}$ reached during washout was significantly larger than prior to the drug application, suggesting that additional hemichannels were recruited during the intervention. At time t=17.5 min, exposure to palmitoleic acid was repeated. Within 3 min, the current components were completely blocked again. Similar observations were made in seven other cells. Exposure to 40 μM 18α-glycyrrhetinic acid, another blocker of gap junction channels (see [13]), yielded similar results (three cells). Conversely, exposure to 60 μM mibefradil, a dose fully blocking I_{VRAC} (see "Pharmacology of I_{VRAC}"), had no effect on I_{hc} (data not shown).

Voltage sensitivity and kinetics of I_{hc}

The bipolar pulses were also used to study the electrical properties of I_{hc}. Starting from V_h=0 mV, V_m was depolarized to 30 mV for 10 s and then hyperpolarized to different levels at increments of 5 to 20 mV (Fig. 9a). The duration of the test pulse varied from 7 to 40 s, enabling I_{hc} to reach a steady state. Figure 9b shows superimposed

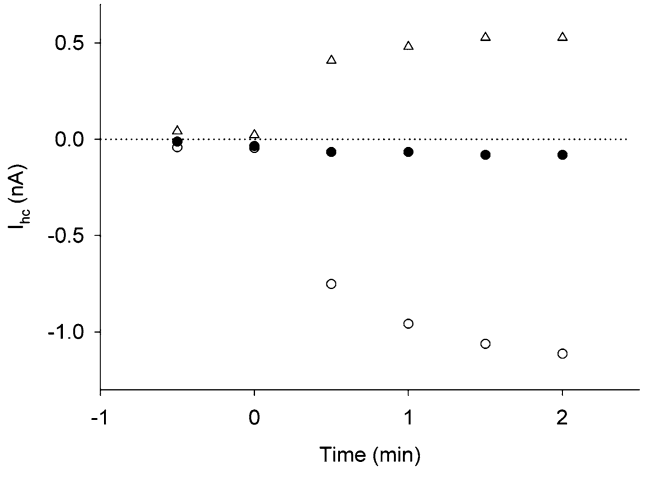

Fig. 7 Effects of low extracellular Ca^{2+} on recruitment of currents carried by Cx45 hemichannels. A bipolar voltage pulse (prepulse: 30 mV, 10 s; test pulse: −40 mV, 5 s) was applied every 30 s to elicit the extra current, I_{hc}. At time t=0 min, solution of normal Ca^{2+} (2 mM) and osmolarity (310 mOsm) was replaced by solution with low Ca^{2+} (~20 nM). The following current components were plotted against time: △, $I_{hc,max}$ (maximal outward current during prepulse); ○, $I_{hc,inst}$ (instantaneous inward current at beginning of test pulse); ●, $I_{hc,ss}$ (steady-state inward current at end of test pulse)

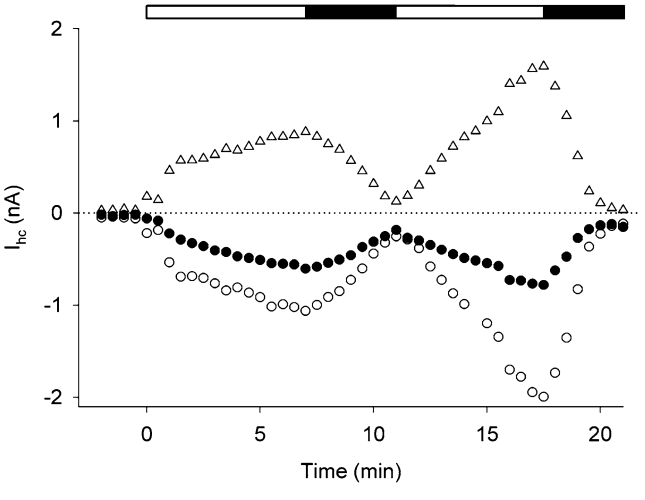

Fig. 8 Pharmacological identification of currents carried by Cx45 hemichannels. Time-course study of current components: △, $I_{hc,max}$ (maximal outward current during prepulse to 30 mV; ○, $I_{hc,inst}$ (instantaneous inward current at beginning of test pulse to −40 mV); ●, $I_{hc,ss}$ (steady-state inward current at end of test pulse). Interventions: time t=0 min, Ca^{2+} in the bath was reduced from 2 mM to ~20 nM; t=7 min, 50 μM palmitoleic acid was washed in; t=11 min, palmitoleic acid was washed out in presence of albumin (1 mg/ml) to speed up recovery

traces indicating that I_{hc} deactivated at negative V_m. Figure 9c shows the current/voltage relationships deduced from the records in Fig. 9b and others from the same experiment, plotting $I_{hc,inst}$ (○) and $I_{hc,ss}$ (●), respectively, as a function of V_m. The $I_{hc,inst}$ data yielded a quasi-linear relationship with deviations towards the *x*-axis at large V_m. In contrast, the $I_{hc,ss}$ data showed a pronounced decrease at negative voltages.

Current records like those in Fig. 9b were then used to establish the voltage dependence of $g_{hc,inst}$ and $g_{hc,ss}$. The result of this analysis has already been communicated [2]. Since it is essential for a comparison with the properties of I_{VRAC}, the procedure is outlined briefly and the data are presented in condensed form. The values of $I_{hc,inst}$ and $I_{hc,ss}$ were used to calculate $g_{hc,inst}$ and $g_{hc,ss}$, respectively. In the case of $g_{hc,inst}$, a value extrapolated to V_m=0 mV served as reference. In the case of $g_{hc,ss}$, the data were expressed as a fraction of $g_{hc,inst}$ of the same pulse. The normalized data were averaged and plotted as a function of V_m. Figure 10a depicts the functions $g_{hc,inst}=f(V_m)$ (dashed line) and $g_{hc,ss}=f(V_m)$ (continuous curve) derived from curve fitting, omitting the data points for clarity (replotted from [2]). The function $g_{hc,inst}=f(V_m)$ was linear and exhibited a small negative slope. The function $g_{hc,ss}=f(V_m)$ was sigmoidal. It showed a maximum at positive and a minimum at negative V_m, leading to a steep transition with a positive slope (Boltzmann parameters: $V_{hc,0}$=−1.08 mV, $g_{hc,max}$=1.04, $g_{hc,min}$=0.08, z=4.0 [2]).

The kinetics of I_{hc} have also been examined before [2]. Again, for comparison with the I_{VRAC} data, the analysis procedure and the deactivation data are summarized briefly. Figure 9b shows that I_{hc} decayed exponentially with time. Curve-fitting yielded the time constants of deactivation, τ_d. Figure 10b shows a plot of the function $\tau_d=f(V_m)$, omitting the data points (replotted from [2]). Over the voltage range

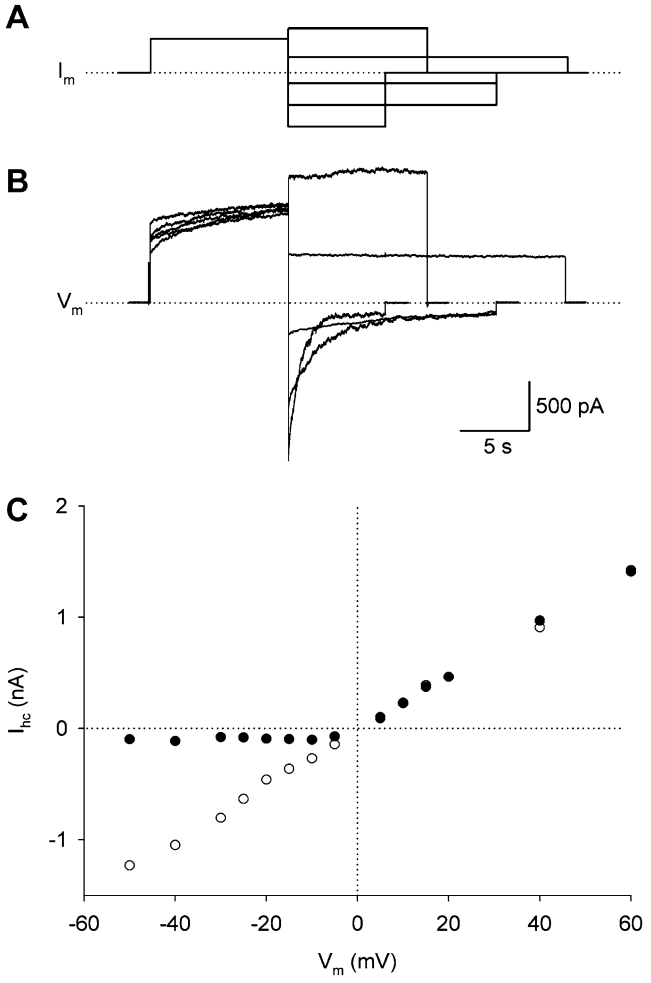

Fig. 9 Voltage dependence of I_{hc}. **a** Bipolar pulse protocol. A depolarizing prepulse from 0 to 30 mV for 10 s was followed by a variable test pulse to negative (−50, −30 and −10 mV) and positive voltage (15 and 40 mV) for 7 to 20 s. **b** Family of associated current traces, I_{hc}. The prepulse resulted in an outward current. Test pulses to negative V_m gave rise to inward currents decaying with time; test pulses to positive V_m led to outward currents of constant amplitude. **c** Plot of instantaneous current, $I_{hc,inst}$ (○), and steady-state current, $I_{hc,ss}$ (●), against V_m

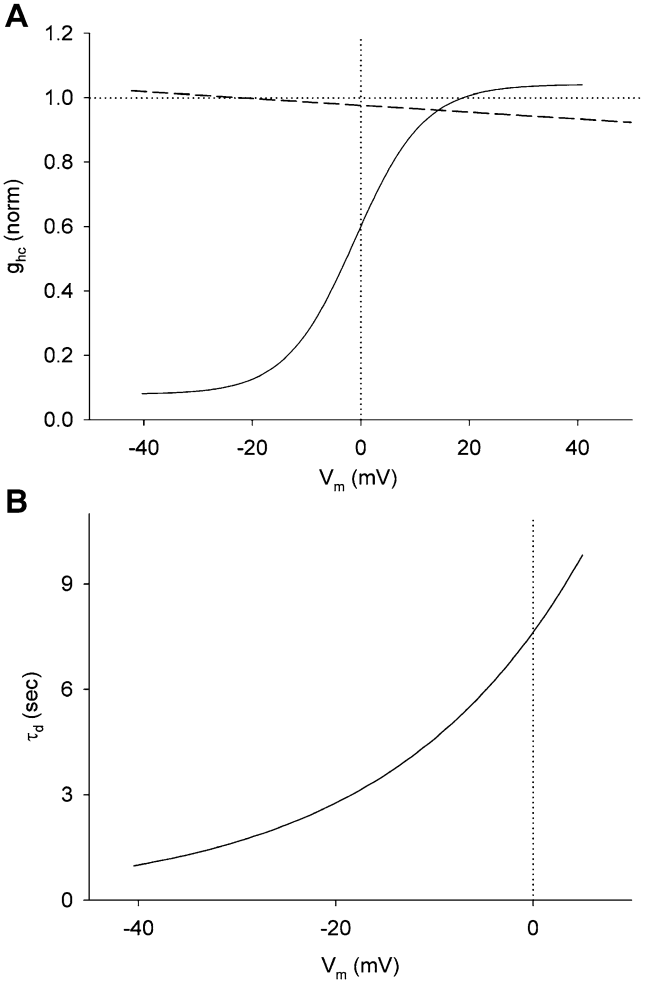

Fig. 10 Conductance and kinetic properties of Cx45 hemichannels. **a** Plot of instantaneous conductance, $g_{hc,inst}$ (*dashed line*), and steady-state conductance, $g_{hc,ss}$ (*continuous curve*), against V_m. Continuous curve: least-squares fit of data to Eq. 2: $V_{hc,0}$=−1.08 mV, $g_{hc,max}$=1.04, $g_{hc,min}$=0.08, z=4.0. **b** Plot of time constant of I_{hc} deactivation, τ_d, against V_m. Continuous curve: least-squares fit of data to Eq. 3: $\tau_{d,0}$=7.6 s (zero V_m intercept), V_τ = 19.7 *mV* (decay constant). Redrawn from [2]. Data points omitted for clarity

from −50 to 5 mV, τ_d increased monotonically as V_m was made less negative. The curve corresponds to the best fit of data to Eq. 3: $\tau_{d,0}$=7.6 s, V_τ = 19.7 mV [2].

Concomitant operation of VRAC and Cx45 hemichannels

When studying I_{VRAC} in appropriate solution (normal Ca^{2+}, reduced osmolarity), $g_{VRAC,max}$ determined at V_m=−50 mV was 16.2±0.6 nS (n=4). When examining I_{hc} in appropriate solution (low Ca^{2+}, normal osmolarity), $g_{hc,max}$ determined at V_m=30 mV was 13.3±2.7 nS (n=8). If one considers the unitary conductance of the respective channels at these voltages, i.e. ~10 and ~53 pS (T. Voets, unpublished, quoted in [18, 27]), this corresponds to 1,600 and 250 operational VRAC and Cx45 hemichannels, respectively.

On the basis of these data and those on V_m dependency of $g_{VRAC,ss}$ and $g_{hc,ss}$ (see Figs. 6a and 10a), an attempt was made to simulate the concomitant presence of I_{VRAC} and I_{hc}. This situation prevailed when I_{hc} was studied with osmotically unbalanced solutions (see "Initial observations"). Figure 11 illustrates the simulation data plotting the absolute values of $g_{m,ss}$ against V_m. The continuous curves a and e represent the functions $g_{VRAC,ss}$=f(V_m) and $g_{hc,ss}$=f(V_m), respectively, calculated from the experimental data (mean values of $g_{VRAC,max}$ and $g_{hc,max}$ given above, and Boltzmann parameters from Figs. 6a and 10a). These functions were then used to compute the behaviour of $g_{m,ss}$ in the case of a simultaneous operation of VRAC and Cx45 hemichannels. The interrupted curves illustrate the conductance functions assuming the following ratios of $g_{VRAC,max}/g_{hc,max}$: 75/25% (b); 50/50% (c); 25/75% (d). They were calculated from the equation

$$g_{m,ss} = f(V_m) = p[g_{m,ss} = f(V_m)]_{VRAC}\} + q[g_{m,ss} = f(V_m)]_{hc}\}, \quad (4)$$

where p and q are the relative weights of $g_{VRAC,max}$ and $g_{hc,max}$, respectively [6]. Instead of sigmoidal, these functions are bell-shaped and exhibit a maximum at V_m≅20 mV. The filled circles connected by solid lines represent the data from an early experiment examining Cx45 hemichannels (see "Initial observations"). The contour of this plot was also bell-shaped. Hence, it resembles those calculated for a simultaneous operation of VRAC and Cx45 hemichannels.

Discussion

Under certain experimental conditions, Cx45-HeLa cells exhibit two complementary currents. One of them is carried by anions (primarily Cl^- in the present context) and deactivates at positive V_m. It is attributable to VRAC (see [18]). The other one is carried by anions and cations (primarily K^+ and Cl^-) and deactivates at negative V_m. It involves Cx45 hemichannels [2, 27]. Concomitant operation of both channels provokes complex currents and may lead to erroneous interpretations.

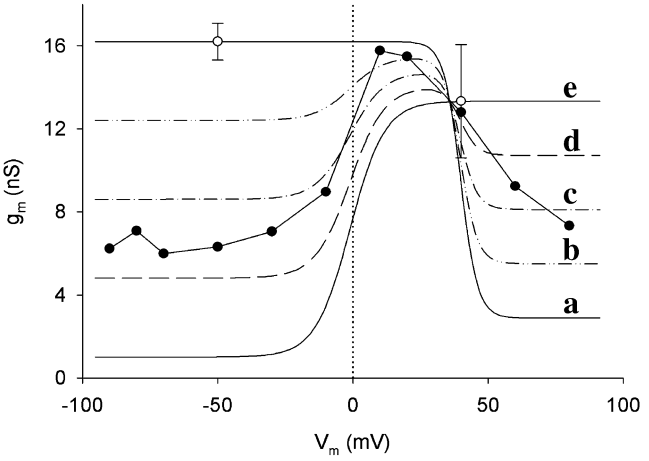

Fig. 11 Simultaneous operation of VRAC and Cx45 hemichannels. Plots of conductance $g_{m,ss}$ against V_m. Continuous curves: functions $g_{VRAC,ss}$=f(V_m) (**a**) and $g_{hc,ss}$=f(V_m) (**e**) gained from separate experiments; ○, mean values of $g_{VRAC,max}$ (16.2±0.6 nS; n=4) and $g_{hc,max}$ (13.3±2.7 nS; n=8). Interrupted curves: computed functions $g_{m,ss}$=f(V_m) for different ratios $g_{VRAC,max}/g_{hc,max}$: 75/25% (**b**), 50/50% (**c**), 25/75% (**d**). Computations are based on curves **a** and **e**. ●, connected by *solid lines*: data from an experiment exploring I_{hc} without precautions to avoid interference from I_{VRAC}

Volume-regulated anion channels

Biophysical characterization To examine currents carried by VRAC, cells were subjected to a mild osmotic intervention, i.e. lowering the osmolarity of the bath solution from 310 to 290 mOsm. This evoked constant inward currents at negative V_m and outward currents with a prominent deactivation at positive V_m (see Fig. 5b). The function $g_{VRAC,inst}$=f(V_m) was slightly sigmoidal and showed a positive slope, while $g_{VRAC,ss}$=f(V_m) was clearly sigmoidal and yielded a negative slope ($V_{m,0}$=39.9 mV, z=8.1; see Fig. 6a). The maximal $g_{VRAC,ss}$ at negative V_m reflects the total number of channels in the open state, and the minimal $g_{VRAC,ss}$ at positive V_m an incomplete deactivation of VRAC and/or a contribution of background currents. The kinetic analyses revealed that I_{VRAC} deactivates exponentially with time at positive V_m, giving rise to single time constants, τ_d (see Fig. 5b). The more positive the V_m, the faster was the deactivation. Over the voltage range yielding reliable data, i.e. 40 to 80 mV, the function τ_d=f(V_m) was exponential (zero V_m intercept $\tau_{d,0}$=317 s, decay constant V_τ = 11.6 mV ; see Fig. 6b). In

conclusion, since VRAC are open at physiological V_m and deactivate at V_m>25 mV, they are expected to affect the properties of non-excitable and excitable membranes, i.e. the resting potential and/or the action potential, despite the small unitary conductance.

Similar *I/V* relations of $I_{VRAC,inst}$ have been reported for different types of cells ([9, 19]; B. Nilius and J. Prenen, unpublished observation, quoted in [18]). However, so far no kinetic data have been made available. Recently, it has been reported that single VRAC exhibit an *I/V* relationship with outward rectification (T. Voets, unpublished, see [18]). This offers an explanation for the non-linear relationship $I_{VRAC,inst}=f(V_m)$. Interestingly, it has been observed that I_{VRAC} decreases in size when cells switch from proliferation to differentiation (see [18]). Moreover, it was found that Cl^- currents alter during the cell cycle, being high in G_1-phase and low in S-phase and increasing again in M-phase [5, 31]. This may explain the variability of I_{VRAC} in our study carried out on cells of non-synchronized cultures.

Replacing Cl^- in the pipette solution against $aspartate^-$, we found a shift of the reversal potential of I_{VRAC} towards positive voltages. This suggests that these channels are more permeable to Cl^- than $aspartate^-$ (see "Voltage sensitivity of I_{VRAC}"). This preference is characteristic for VRAC channels (see [18]).

Ionic characterization An odd current appeared occasionally when Cx45-HeLa cells were exposed to solutions aimed at examining I_{hc} (see "Initial observations"). It turned out that this was caused by osmotic perturbations. When cells were grown in the incubator, the osmolarity of the medium increased gradually (~3% per day). Subsequent exposure to salt solutions introduced an osmotic stress which caused cell swelling via water influx and activation of VRAC (see [18]). Such small osmotic shifts were sufficient to evoke I_{VRAC}.

Pharmacological characterization Mibefradil is a useful tool to block VRAC [18, 20]. We found that it inhibited I_{VRAC} in a dose-dependent and reversible manner (see Fig. 4). It had no effect on Cx45 hemichannels. Hence, 60 μM mibefradil was routinely added to the bath solution when I_{hc} was examined (see "Cx45 hemichannels"). Conversely, I_{VRAC} was not affected by 40 μM 18α-glycyrrhetinic acid and only weakly impaired by 50 μM palmitoleic acid, doses which fully block gap junction channels and hemichannels (see [13]).

Cx45 hemichannels

Biophysical characterization To study currents carried by Cx45 hemichannels, I_{hc}, cells were exposed to low-Ca^{2+} solution. This evoked a current whose voltage sensitivity was a mirror image of I_{VRAC} (see Fig. 9). Depolarization gave rise to outward currents which activated slowly with time; hyperpolarization yielded inward currents with a prominent deactivation. The function $g_{hc,inst}=f(V_m)$ was linear and exhibited a negative slope, while $g_{hc,ss}=f(V_m)$ was sigmoidal and grew with positive V_m (Boltzmann parameters: $V_{hc,0}$=−1.08 mV, z=4.0; see Fig. 10a). The maximal $g_{hc,ss}$ at positive V_m corresponds to the channels in the open state, and the minimal $g_{hc,ss}$ at negative V_m to incomplete channel closure and/or incomplete deactivation of I_{hc} [2]. However, a contribution of background currents cannot be excluded. A recent study on Cx45 hemichannels reported a similar relationship $g_{hc,ss}=f(V_m)$ [27]. Comparison of $I_{hc,ss}$ and $I_{VRAC,ss}$ data indicates that gating of Cx45 hemichannels is less voltage-sensitive than gating of VRAC. The kinetic studies revealed that I_{hc} deactivates exponentially with time, giving rise to single time constants, τ_d. The more negative the V_m, the more rapid was the deactivation. Over the range of V_m which yielded reliable data, i.e. −40 to 5 mV, the function $\tau_d=f(V_m)$ was exponential ($\tau_{d,0}$=7.6 s, V_τ = 19.7 mV; see Fig. 10b). Hence, deactivation of I_{hc} is less voltage-sensitive than deactivation of I_{VRAC}. In conclusion, since most Cx45 hemichannels are in the residual state at physiological V_m [27], they are likely to have a small effect on the properties of non-excitable and excitable membranes. Nonetheless, few open channels of a sizable unitary conductance may already affect V_m.

It has been reported that the unitary currents of Cx45 hemichannels are voltage-sensitive [27]. This suggests that the negative slope of the function $g_{hc,inst}=f(V_m)$ is an intrinsic property of Cx45 hemichannels.

Ionic characterization To activate a maximal number of Cx45 hemichannels, $[Ca^{2+}]_o$ had to be reduced from 2 mM to ~20 nM (P. Bader, R. Weingart and M. Egger, in preparation). This finding differs from a recent study on Cx45 hemichannels performed in solution nominally free of Ca^{2+} [27]. Without precautions, such solutions have a free $[Ca^{2+}]\geq$10 μM [17], a value much larger than $[Ca^{2+}]_o$ used in our experiments. This difference may contribute to the larger $g_{hc,max}$ found in the present study (13.3 vs 5.9 nS). If we assume that Cx45 gap junction channels exhibit a Ca^{2+} sensitivity similar to that of other gap junction channels (see [13]), this suggests that Cx45 hemichannels are more sensitive to Ca^{2+} than Cx45 gap junction channels. Alternatively, Cx45 gap junction channels and hemichannels may be more sensitive to Ca^{2+} than other channels and hemichannels.

A recent paper reported that osmotic stress, like metabolic inhibition, elicited a current carried by Cx43 hemichannels [14]. In light of our data, this raises the question whether the current evoked was carried by VRAC rather than hemichannels.

Pharmacological characterization Palmitoleic acid blocks gap junction channels [4]. It inhibited Cx45 hemichannels

in a dose-dependent manner; complete block of I_{hc} was obtained at 50 μM (see Fig. 8). I_{hc} was also inhibited by 40 μM 18α-glycyrrhetinic acid which acts on gap junction channels and hemichannels (see [13]). In contrast, Cx45 hemichannels were not affected by mibefradil up to 60 μM (see "Pharmacology of I_{hc}" in "Results"). Recently, it has been reported that some Cl^- channel blockers, i.e. flufenamic acid and NPPB, also inhibit Cx50 and Cx46 hemichannels [12]. Since the latter agent also blocks VRAC (see [18]), caution is suggested when mibefradil is used for hemichannel studies.

Concurrent operation of VRAC and Cx45 hemichannels

VRAC and Cx45 hemichannels have similar and dissimilar properties. VRAC are outward rectifying and deactivate at positive V_m; Cx45 hemichannels are inward rectifying and deactivate at negative V_m. In both cases, the current decreases with an exponential time-course. Hence, the gating mechanisms resemble each other, but respond to opposite polarity. Moreover, the single-channel conductance is voltage-sensitive, yet the size is different (~25 and 60 pS, extrapolated to V_m=0 mV; see [18] and [27]).

What are the implications when VRAC and hemichannels are involved simultaneously? Provided that hemichannels are gating with negative voltage, this results in a shallow bell-shaped function $g_{m,ss}=f(V_m)$. This situation prevailed when Cx45 hemichannels were examined under osmotic stress (see Fig. 11). However, it could also be interpreted as behaviour of a single type of hemichannel (see [28]). Assuming that hemichannels are gating with positive voltage, this leads to an S-shaped function $g_{m,ss}=f(V_m)$ of negative slope. Hence, participation of two types of channels may not be obvious, even when using pharmacology. Interestingly, beyond this interaction, there is a possibility that VRAC and hemichannels are recruited sequentially under certain conditions. Based on the properties of these channels, we propose the following scheme. Hypotonic stress leads to cell swelling, opening of VRAC and subsequent release of nucleotides such as ATP^{2-} (see [18]). This in turn provokes opening of gap junction hemichannels [14] and closure of gap junction channels [25]. This pathway may be activated under physiological (e.g. cell proliferation, shear stress, secretion of fluid by glandular cells) as well as pathophysiological situations (e.g. ischaemia, congestive heart failure, hepatic cirrhosis). As suggested before (see [18]), ATP^{2-} released may then be involved in mediating autocrine/paracrine signaling via purinergic receptors.

Acknowledgements We thank D. Lüthi for technical assistance and B. Nilius, University of Leuven, Belgium, for suggesting the use of mibefradil. Transfectants were provided by K. Willecke, Institute of Genetics, University of Bonn, Germany. Supported by the Swiss National Science Foundation (31-55297.98, 31-67230.01).

References

1. Bader P, Weingart R (2003) Pitfalls in examining connexin hemichannels. In: Proceedings of the 2003 International Gap Junction Conference, Cambridge, UK, 23–28 August, p 41
2. Bader P, Weingart R (2004) Conductive and kinetic properties of connexin45 hemichannels expressed in transfected HeLa cells. J Membr Biol 199:143–154
3. Bittman KS, Lo Turco JJ (1999) Differential regulation of connexin 26 and 43 in murine neocortical precursors. Cereb Cortex 9:188–195
4. Burt JM, Massey KD, Minnich BN (1991) Uncoupling of cardiac cells by fatty acids: structure–activity relationships. Am J Physiol Cell Physiol 260:C439–C448
5. Chen L, Wang L, Zhu L, Nie S, Zhang J, Zhong P, Cai B, Luo H, Jacob TJC (2002) Cell cycle-dependent expression of volume-activated chloride currents in nasopharyngeal carcinoma cells. Am J Physiol Cell Physiol 283:C1313–C1323
6. Desplantez T, Weingart R (2004) Cardiac connexins Cx43 and Cx45: formation of diverse gap junction channels with diverse electrical properties. Pflügers Arch 448:363–375
7. De Vries SH, Schwartz EA (1992) Hemi-gap junction channels in solitary horizontal cells of the catfish retina. J Physiol (Lond) 445:201–230
8. Díaz M, Sepúlveda FV (1995) Characterization of Ca^{2+}-dependent inwardly rectifying K^+ currents in HeLa cells. Pflügers Arch 430:168–180
9. Díaz M, Valverde MA, Higgins CF, Rucareanu C, Sepúlveda FV (1993) Volume-activated chloride channels in HeLa cells are blocked by verapamil and dideoxyforskolin. Pflügers Arch 422:347–353
10. Ebihara L, Berthoud VM, Beyer EC (1995) Distinct behavior of connexin56 and connexin46 gap junction channels can be predicted from the behavior of their hemi-gap-junctional channels. Biophys J 68:1796–1803
11. Elfgang C, Eckert R, Lichtenberg-Fraté H, Butterweck A, Traub O, Klein RA, Hülser DF, Willecke K (1995) Specific permeability and selective formation of gap junction channels in connexin-transfected HeLa cells. J Cell Biol 129:805–817
12. Eskandari S, Zampighi GA, Leung DW, Wright EM, Loo DDF (2002) Inhibition of gap junction hemichannels by chloride channel blockers. J Membr Biol 185:93–102
13. Harris AL (2001) Emerging issues of connexin channels: biophysics fills the gap. Quart Rev Biophys 34:325–472
14. John S, Cesario D, Weiss JN (2003) Gap junction hemichannels in the heart. Acta Physiol Scand 179:23–31
15. Kamermans M, Fahrenfort I, Schultz K, Janssen-Bienhold U, Sjoerdsma T, Weiler R (2001) Hemichannel-mediated inhibition in the outer retina. Science 292:1178–1180
16. Li H, Liu TF, Lazrak A, Peracchia C, Goldberg GS, Lampe PD, Johnson RG (1996) Properties and regulation of gap junction hemichannels in the plasma membranes of cultured cells. J Cell Biol 134:1019–1030
17. McGuigan JAS, Lüthi D, Buri A (1991) Calcium buffer solutions and how to make them: a do it yourself guide. Can J Physiol Pharmacol 69:1733–1749
18. Nilius B, Droogmans G (2003) Amazing chloride channels: an overview. Acta Physiol Scand 177:119–147
19. Nilius B, Sehrer J, Viana F, De Greef C, Raeymaekers L, Eggermont J, Droogmans G (1994) Volume-activated Cl^- currents in different mammalian non-excitable cell types. Pflügers Arch 428:364–371
20. Nilius B, Prenen J, Voets T, Eggermont J, Droogmans G (1998) Activation of volume-regulated chloride currents by reduction of intracellular ionic strength in bovine endothelial cells. J Physiol (Lond) 506(2):353–361
21. Sauvé R, Roy G, Payet D (1983) Single channel K^+ currents from HeLa cells. J Membr Biol 74:41–49

22. Sauvé R, Simoneau C, Monette R, Roy G (1986) Single-channel analysis of the potassium permeability in HeLa cancer cells: evidence for a calcium-activated potassium channel of small unitary conductance. J Membr Biol 92:269–282
23. Segretain D, Falk MM (2004) Regulation of connexin biosynthesis, assembly, gap junction formation, and removal. Biochim Biophys Acta 1662:3–21
24. Stout CE, Costantin JL, Naus CC, Charles AC (2002) Intercellular calcium signaling in astrocytes via ATP release through connexin hemichannels. J Biol Chem 277:10482–10488
25. Sugiura H, Toyama J, Tsuboi N, Kamiya K, Kodama I (1990) ATP directly affects junctional conductance between paired ventricular myocytes isolated from guinea pig heart. Circ Res 66:1095–1102
26. Trexler EB, Bennett MVL, Bargiello TA, Verselis VK (1996) Voltage gating and permeation in a gap junction hemichannel. Proc Natl Acad Sci U S A 93:5836–5841
27. Valiunas V (2002) Biophysical properties of connexin-45 gap junction hemichannels studied in vertebrate cells. J Gen Physiol 119:147–164
28. Valiunas V, Weingart R (2000) Electrical properties of gap junction hemichannels identified in transfected HeLa cells. Pflügers Arch 440:366–379
29. Valiunas V, Manthey D, Vogel R, Willecke K (1999) Biophysical properties of mouse connexin30 gap junction channels studied in transfected human HeLa cells. J Physiol 519(3):631–644
30. Valiunas V, Weingart R, Brink PR (2000) Formation of heterotypic gap junction channels by connexins 40 and 43. Circ Res 86:e42–e49
31. Zheng YJ, Furukawa T, Tajimi K, Inagaki N (2003) Cl^- channel blockers inhibit transition of quiescent (G_0) fibroblasts into the cell cycle. J Cell Physiol 194:376–383